

Article

Steam Reforming of Bio-Ethanol to Produce Hydrogen over Co/CeO₂ Catalysts Derived from Ce_{1-x}Co_xO_{2-y} Precursors

Yanyong Liu *, Kazuhisa Murata and Megumu Inaba

Research Institute of Energy Frontier, National Institute of Advanced Industrial Science and Technology, AIST, Tsukuba West, Onogawa 16-1, Tsukuba, Ibaraki 305-8569, Japan; kazu-murata@aist.go.jp (K.M.); mg.inaba@aist.go.jp (M.I.)

* Correspondence: yy.ryuu@aist.go.jp; Tel.: +81-29-861-4826; Fax: +81-29-855-0815

Academic Editors: Rafael Luque, Sudipta De and Alina M. Balu

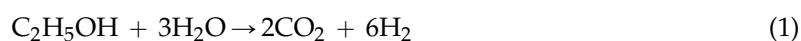
Received: 13 November 2015; Accepted: 27 January 2016; Published: 5 February 2016

Abstract: A series of Ce_{1-x}Co_xO_{2-y} precursors were prepared by homogeneous precipitation using urea as a precipitant. The Co/CeO₂ catalysts obtained from the Ce_{1-x}Co_xO_{2-y} precursors were used for the steam reforming of ethanol to produce hydrogen. Co ions could enter the CeO₂ lattices to form Ce_{1-x}Co_xO_{2-y} mixed oxides at $x \leq 0.2$ using the homogeneous precipitation (hp) method. CeO₂ was an excellent support for Co metal in the steam reforming of ethanol because a strong interaction between support and metal (SISM) exists in the Co/CeO₂ catalysts. Because Co/CeO₂ (hp) prepared by homogeneous precipitation possessed a high BET surface area and small Co metal particles, Co/CeO₂ (hp) showed a higher ethanol conversion than the Co/CeO₂ catalysts prepared using the co-precipitation (cp) method and the impregnation (im) method. The selectivity of CO₂ over Co/CeO₂ (hp) increased with increasing reaction temperature at from 573 to 673 K, and decreased with increasing reaction temperature above 673 K due to the increase of CO formation. The carbonaceous deposits formed on the catalyst surface during the reaction caused a slow deactivation in the steam reforming of ethanol over Co/CeO₂ (hp). The catalytic activity of the used catalysts could be regenerated by an oxidation-reduction treatment, calcined in air at 723 K and then reduced by H₂ at 673 K.

Keywords: bio-ethanol; steam reforming; hydrogen; urea hydrolysis; homogeneous precipitation; Co/CeO₂ catalyst; Ce_{1-x}Co_xO_{2-y} mixed oxide; solid-phase crystallization

1. Introduction

Biomass-derived ethanol (so-called as bio-ethanol) is a renewable fuel because it can be produced by fermentation of biomass, such as starch, sugar, crop wastes, and so on. The concentration of ethanol is 12–15 wt. % in bio-ethanol by the fermentation of biomass. In using bio-ethanol as an additive to gasoline, high energy intensive and rather expensive processes have been used for recovering highly concentrated ethanol (>99.5 wt. %) due to the co-boiling of ethanol and water. On the other hand, hydrogen is an efficient and clean energy and is predicted to become a major source of energy in the future. Hydrogen can be produced by the steam reforming of ethanol (Equation (1)) and this reaction can be used in fuel cell systems [1–3].



As shown in Equation (1), the molar ratio of ethanol to water is three and thus the concentration of ethanol in the mixed solution is about 46 wt. %. Because a 46 wt. % ethanol aqueous is easy to be

obtained by the simple distillation of bio-ethanol, the steam reforming of bio-ethanol (aqueous solution of ethanol) to produce hydrogen has been proposed to be an effective method for the utilization of bio-ethanol fuel.

Base metals (such as Co, Ni, and Cu) and noble metals (such as Rh, Au, and Ir) have been used as the active metal catalysts for ethanol steam [3–25]. Among them, Co is an attractive active metal due to its high catalytic performance and low price. The oxide support plays a significant role in the performance of metal catalysts for ethanol steam. CeO₂ is an excellent support for the metal catalysts in the steam reforming of ethanol. Moreover, the synthesis method greatly influences the catalytic performance of a metal-supported catalyst. Impregnation and co-precipitation are the methods usually to be used for preparing CeO₂-supported metal catalysts in the steam reforming of ethanol. On the other hand, the homogeneous precipitation method by urea hydrolysis has been reported as an excellent method for preparing Cu/ZnAlO catalyst in the steam reforming of methanol and the gas-shift reaction [26,27]. Moreover, the solid-phase crystallization (SPC) method using multi-component precursors is an effective method for synthesizing highly active metal-supported catalysts [28]. We have used the concept of SPC method to prepare active catalysts for some important reactions [29–38]. In this study, we synthesized the Co/CeO₂ catalysts derived from Ce_{1-x}Co_xO_{2-y} precursors by the homogeneous precipitation for the steam reforming of ethanol to produce hydrogen.

2. Results and Discussion

2.1. Catalyst Characterization

Figure 1 shows the X-ray diffraction patterns of Ce_{1-x}Co_xO_{2-y} prepared by homogeneous precipitation after calcination at 723 K for 3 h. The CeO₂ support showed four main reflections corresponding to the (111), (200), (220) and (311) crystallographic planes, implying that the CeO₂ support had a fluorite structure with cubic (fcc) cells. A Co₃O₄ phase ((111) crystallographic plane) appeared at 36.9° in the patterns of the Ce_{1-x}Co_xO_{2-y} mixed oxides when *x* was larger than 0.2, and the intensity of the Co₃O₄ peak increased with increasing Co content in the samples.

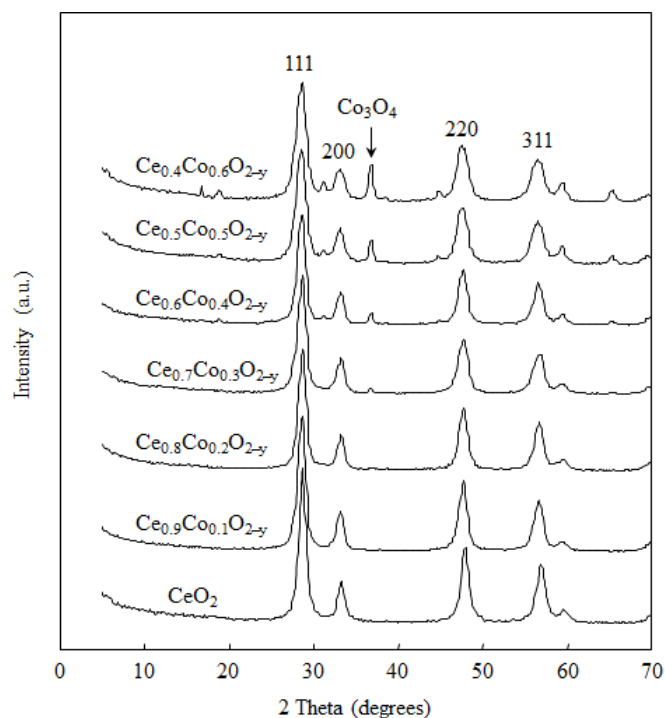


Figure 1. X-ray diffraction patterns of Ce_{1-x}Co_xO_{2-y} prepared by homogeneous precipitation after calcination at 723 K for 3 h.

Figure 2 shows the lattice constant of CeO₂ in the Ce_{1-x}Co_xO_{2-y} prepared by homogeneous precipitation after calcination at 723 K for 3 h. The lattice constants of the CeO₂-based materials were calculated based on the four main reflections in the XRD patterns. The lattice constant of CeO₂ was 0.5410 nm without Co addition. The lattice constant of CeO₂ decreased when Co was added, but almost remained constant (around 0.5354 nm) when x was larger than 0.2 in the Ce_{1-x}Co_xO_{2-y} mixed oxides. These results indicated that the smaller Co ions could enter in the CeO₂ lattice to form a homogeneous Ce_{1-x}Co_xO_{2-y} solid solution at $x \leq 0.2$. For the Ce_{1-x}Co_xO_{2-y} samples with $x > 0.2$, a part of Co ions entered in the CeO₂ lattice to form a solid solution and the remaining Co ions formed large Co₃O₄ particles on the surface of CeO₂.

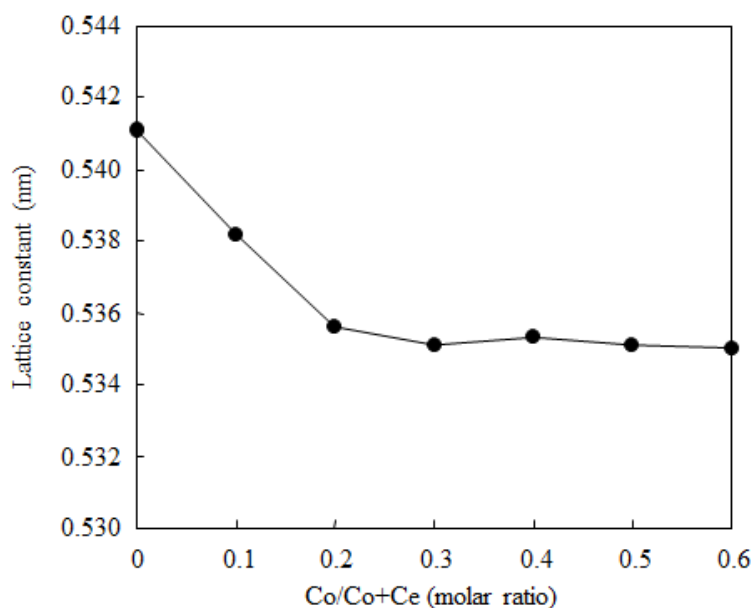


Figure 2. Lattice constant of CeO₂ in the Ce_{1-x}Co_xO_{2-y} prepared by homogeneous precipitation after calcination at 723 K for 3 h.

Table 1 summarizes the physical properties of various Co-supported catalysts with 7.7 wt. % Co loading. All samples were reduced in H₂ at 673 K for 10 h. The actual Co loadings, which were measured by ICP elemental analysis, were very similar to the Co loadings designed in the catalysts.

Table 1. Physical characters of various Co-supported catalysts with 7.7 wt. % Co loading.

Sample	BET Surface Area (m ² ·g ⁻¹)	Co Particle Size (nm) ^a	Co Dispersion Degree (%) ^a
Co/CeO ₂ (hp)	135	7.6	12.6
Co/CeO ₂ (cp)	102	9.5	10.1
Co/CeO ₂ (im)	88	17.7	5.4
Co/Al ₂ O ₃ (im)	147	14.3	6.7

^a Obtained by CO adsorption.

The 7.7 wt. % Co/CeO₂ (hp) catalyst obtained by reducing the Ce_{0.8}Co_{0.2}O_{2-y} precursor showed a BET surface area of 135 m²·g⁻¹, which was higher than those of Co/CeO₂ (cp) (102 m²·g⁻¹) and Co/CeO₂ (im) (88 m²·g⁻¹). Co ions were doped in the CeO₂ positions in the Ce_{0.8}Co_{0.2}O_{2-y} precursor, which caused a decrease in the crystallization degree of CeO₂-based support. Further, the decrease of the crystallization degree could cause an increase of the BET surface area in Co/CeO₂ (hp). The Co particles' size measured by CO absorption was 7.6, 9.5, and 17.7 nm for Co/CeO₂ (hp), Co/CeO₂ (cp), and Co/CeO₂ (im), respectively. The use of multi-component precursors may yield well-dispersed metal particles on the surface of supports after calcination and reduction; this property, known as

solid-phase crystallization (SPC), is important in the preparation of highly active metal-supported catalysts [27–33]. Using the homogeneous precipitation, Co ions could enter in the CeO_2 lattice to form a $\text{Ce}_{1-x}\text{Co}_x\text{O}_{2-y}$ solid solution after calcination in air at 723 K. On the other hand, Co ions could not enter in the CeO_2 lattice using the impregnation, which caused the large Co particles to be formed in Co/CeO_2 (im).

Figure 3 shows the H_2 -TPR profiles of various Co-based samples after calcination at 723 K for 3 h. The Co loading was 7.7 wt. % for each sample. H_2 -TPR is a useful tool to trace the reduction of the oxide phases. The Co_3O_4 particles formed on the support surface upon calcination are very difficult to be reduced to active Co^0 species in the H_2 flow [11,39]. In Figure 3, all samples showed the reduction peaks at low temperature (with the maximum at about 513 K) assigning to the reduction of $\text{Co}^{3+} \rightarrow \text{Co}^{2+}$ and at high temperature (from 563 to 723 K) assigning to the reduction of $\text{Co}^{2+} \rightarrow \text{Co}^0$. Moreover, the reduction of $\text{Co}^{2+} \rightarrow \text{Co}^0$ contained two unseparated peaks for each sample due to the stepwise reduction steps of various Co^{2+} species absorbed on the supports [11,39,40]. The reduction temperature of Co_3O_4 on various catalysts followed the order of Co/CeO_2 (hp) < Co/CeO_2 (cp) < Co/CeO_2 (im) < $\text{Co}/\text{Al}_2\text{O}_3$ (im). The catalysts were pretreated in H_2 flow at 673 K (for 10 h) in this study in order to avoid the severe sintering of Co particles at high reduction temperature. As shown in Figure 3, the reduction peak of $\text{Co}^{2+} \rightarrow \text{Co}^0$ (H) (strong absorbed Co^{2+} to Co^0) in the H_2 -TPR profiles of $\text{Co}/\text{Al}_2\text{O}_3$ (im) and Co/CeO_2 (im) reached over 673 K, which means that some Co^{2+} species in $\text{Co}/\text{Al}_2\text{O}_3$ (im) and Co/CeO_2 (im) could not be reduced to active Co^0 species under the pretreatment condition in this study (H_2 reduction at 673 K).

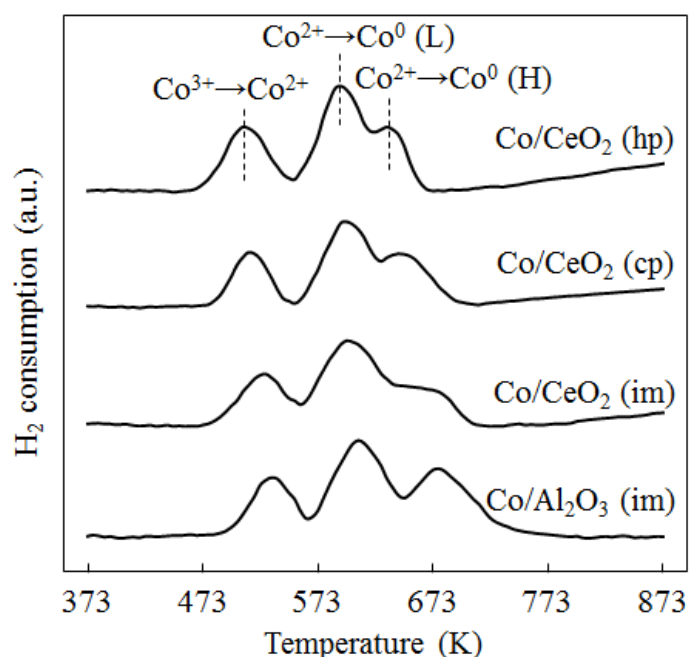


Figure 3. H_2 -TPR profiles of various Co-based samples after calcination at 723 K for 3 h.

Figure 4 shows the TEM image of 7.7 wt. % Co/CeO_2 (hp) catalyst. The sample was pre-reduced in H_2 at 673 K for 10 h. The particle size of CeO_2 from the TEM image is about 10 nm, which is consistent with the size of the CeO_2 particles calculated from the XRD pattern. Moreover, the CeO_2 particles are distributed uniformly, which is an advantage of the homogeneous precipitation method for preparing catalysts. Because the size of the Co particles (7.6 nm from CO adsorption) is similar to the size of the CeO_2 particles (about 10 nm from XRD pattern) in the 7.7 wt. % Co/CeO_2 (hp) catalyst, it is difficult to distinguish Co particles from CeO_2 particles in the TEM image.

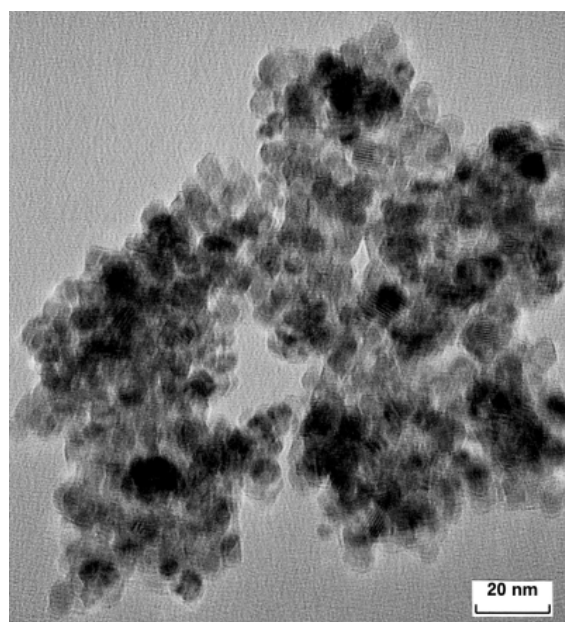


Figure 4. TEM image of 7.7 wt. % Co/CeO₂ (hp) catalyst.

2.2. Catalyst Activity

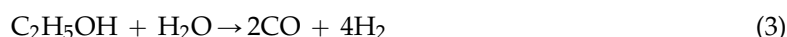
Table 2 summarizes the reaction results over various catalysts for the steam reforming of ethanol at 673 K. Co/Al₂O₃ (imp) showed a low conversion of 25.5% at 673 K. A relatively large amount of C₂H₄ was formed over Co/Al₂O₃ (im) because the acidity of Al₂O₃ support caused the dehydration of ethanol. Co/CeO₂ (im) showed an ethanol conversion (40.3%) much higher than that over Co/Al₂O₃ (im) (25.5%) prepared by the same impregnation method. This indicates that CeO₂ is an effective support for Co metal in the steam reforming of ethanol. The CeO₂-supported catalysts possess strong interaction between support and metal (SISM) during the reaction [41]. The SISM effect gave the CeO₂-supported metal catalysts high activities for many reactions [29–43]. The synthesis method greatly influences the catalytic performance of Co/CeO₂ catalysts for the steam reforming of ethanol. The Co/CeO₂ (hp) catalyst showed a conversion of 85.9%, which was much higher than those over Co/CeO₂ (cp) (68.4%) and Co/CeO₂ (im) (40.3%) with the same Co loading under the same reaction conditions. Use of multi-component precursors may give well-dispersed metal particles on the surface of supports after calcination and reduction, which is called as solid-phase crystallization (SPC) method for preparing highly active metal-supported catalysts [27–33]. For Co/CeO₂ (hp) catalyst, Co ions were introduced into the CeO₂ framework to form Ce_{0.8}Co_{0.2}O_{2-y} precursor after calcination. Therefore, after reducing Ce_{0.8}Co_{0.2}O_{2-y} solid solution in H₂, Co metal particles uniformly formed on the CeO₂ surface and strongly interact with the CeO₂ support. As shown in Table 2, Co/CeO₂ (hp) obtained the largest ethanol conversion and the largest selectivity to CO₂ among various catalysts, which meant that the H₂ yield of Co/CeO₂ (hp) was much higher than other catalysts.

Table 2. Reaction results over various catalysts for the steam reforming of ethanol at 673 K ^a.

Catalyst ^b	Conversion of Ethanol (%)	Selectivity to C-products (%)					H ₂ Yield (Molar Ratio of [H ₂] _{out} /[EtOH] _{in})
		CO ₂	CO	CH ₄	C ₂ H ₄	OC ^c	
Co/Al ₂ O ₃ (im)	25.5	54.9	19.5	8.3	13.9	3.3	1.1
Co/CeO ₂ (im)	40.3	70.6	15.2	4.4	3.7	4.8	2.1
Co/CeO ₂ (cp)	68.4	73.3	14.6	3.7	2.8	4.3	3.6
Co/CeO ₂ (hp)	85.9	76.2	12.1	3.5	3.1	4.2	4.7

^a Catalyst amount: 1 g; C₂H₅OH: 17 mL·min⁻¹; H₂O: 50 mL·min⁻¹; N₂: 17 mL·min⁻¹. ^b Co loading: 7.7 wt. %. ^c OC: oxygenated compounds, including CH₃CHO, CH₃COCH₃, and so on.

The main C-containing products of the steam reforming of ethanol are CO_2 , CO , C_2H_4 , CH_4 , CH_3CHO , and CH_3COCH_3 . CO_2 is formed by the steam reforming of ethanol (Equation (1)) and the water-gas shift reaction (Equation (2)). There are several ways to form CO : the ethanol steam reforming to syngas (Equation (3)); the ethanol cracking (Equation (4)), and the reverse water-gas shift reaction (Equation (5)). CH_4 is formed by the ethanol cracking (Equation (4)). C_2H_4 is formed by the ethanol dehydration (Equation (6)). Acetaldehyde is the main oxygenated compound and it is formed by the ethanol dehydrogenation (Equation (7)). Acetone is formed by the acetaldehyde decomposition (Equation (8)). The largest value of H_2 yield (molar ratio of $[\text{H}_2]_{\text{out}}/[\text{EtOH}]_{\text{in}}$) is six when both the $\text{C}_2\text{H}_5\text{OH}$ conversion and the selectivity to CO_2 are 100% in the steam reforming of ethanol (Equation (1)). The H_2 yield decreases when the side-reactions (Equations (2)–(8)) occur during the reaction.



As shown in Table 2, compared to the $\text{Co}/\text{Al}_2\text{O}_3$ (im) catalyst, the Co/CeO_2 (im) catalyst formed a less amount of C_2H_4 because the basicity of CeO_2 support suppressed the ethanol dehydration (Equation (6)). Moreover, because CeO_2 support has high oxygen storage capacity, the ethanol decomposition (Equation (4)) was suppressed in the Co/CeO_2 catalysts by transferring mobile oxygen species to Co from CeO_2 [24]. Hence, the amounts of CO and CH_4 formed over Co/CeO_2 (im) were less than those formed over $\text{Co}/\text{Al}_2\text{O}_3$ (im) during the reaction.

Figure 5 shows the effect of Co loading in the Co/CeO_2 (hp) catalyst for the steam reforming of ethanol at 673 K. The reaction conditions are the same as those in Table 2. The ethanol conversion increased with increasing Co loading and showed the maximum value at a 17.4 wt. % Co loading (precursor: $\text{Ce}_{0.6}\text{Co}_{0.4}\text{O}_{2-y}$). However, the ethanol conversion did not show an obvious increase at above 7.7 wt. % Co loading in the Co/CeO_2 (hp) catalyst.

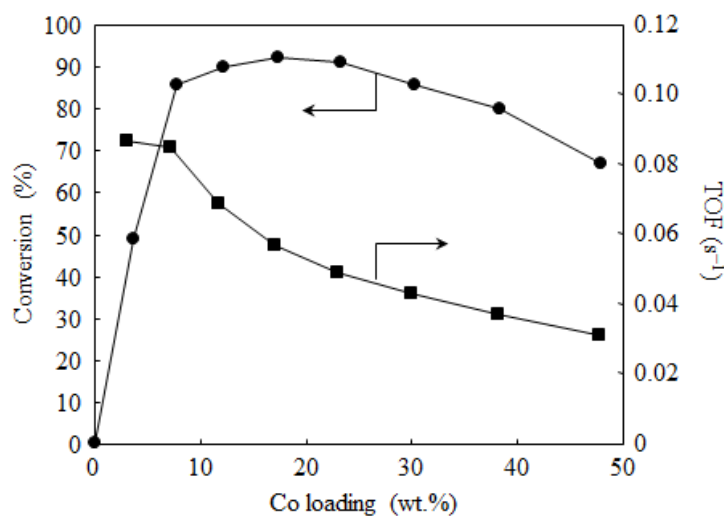


Figure 5. Effect of Co loading in the Co/CeO_2 (hp) catalyst for the steam reforming of ethanol at 673 K.

The turnover frequency (TOF) was defined as the number of converted ethanol molecules per Co surface site per second. In Figure 5, the TOF value was calculated from the number of metallic Co atoms (measured by CO chemisorption) and the rate of the convert C_2H_5OH atoms at 673 K over the Co/CeO₂ (hp) catalyst. The TOF values decreased with increasing Co loading in the Co/CeO₂ (hp) catalyst. The TOF value of 7.7 wt. % Co/CeO₂ (hp) (precursor: Ce_{0.8}Co_{0.2}O_{2-y}) was just slightly lower than that of 3.6 wt. % Co/CeO₂ (hp) (precursor: Ce_{0.9}Co_{0.1}O_{2-y}). However, the TOF value of 12.2 wt. % Co/CeO₂ (hp) (precursor: Ce_{0.7}Co_{0.3}O_{2-y}) greatly decreased as compared with that of 7.7 wt. % Co/CeO₂ (hp). There was a limitation of the Co capacity entered in the CeO₂ lattice in Ce_{1-x}Co_xO_{2-y}. The Co ions which did not dissolve into the CeO₂ lattices formed large Co particles after reduction and the activity of large Co particles was low for the steam reforming of ethanol. The Co ions could not dissolve into the CeO₂ lattice completely in the Ce_{0.7}Co_{0.3}O_{2-y} precursor, which caused a large decrease in the TOF value over the 12.2 wt. % Co/CeO₂ (hp) catalyst.

Figure 6 shows the effect of reaction temperature on the ethanol conversion over various catalysts. The reaction conditions are the same as those in Table 2. For the reaction without a catalyst, the ethanol conversion was very low (<5%) even at a high reaction temperature of 773 K. At the same reaction temperature, the conversion over each catalyst with a 7.7 wt. % Co loading was in an order of Co/CeO₂ (hp) > Co/CeO₂ (cp) > Co/CeO₂ (im) > Co/Al₂O₃ (im). By using the Co/CeO₂ (hp) catalyst derived from Ce_{1-x}Co_xO_{2-y} precursor, a high ethanol conversion had been achieved at a low temperature for the steam reforming of ethanol.

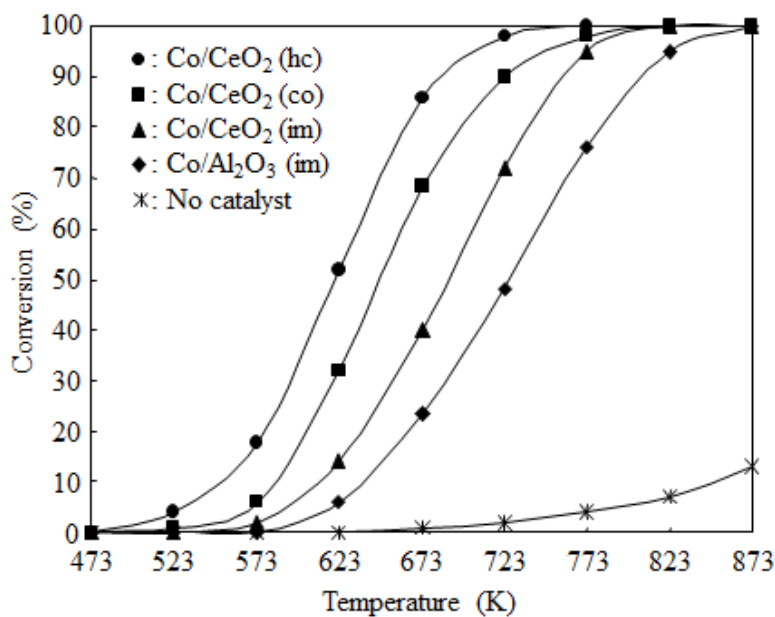


Figure 6. Effect of reaction temperature on the ethanol conversion over various catalysts.

Figure 7 shows the effect of reaction temperature on the selectivity to C-containing products over 7.7 wt. % Co/CeO₂ (hp). The reaction conditions are the same as those in Table 2. The selectivity to CH₄ did not show a large change at various reaction temperatures. Both the selectivity to oxygenated compounds and the selectivity to C₂H₄ decreased with increasing reaction temperature. On the other hand, the selectivity to CO increased with increasing reaction temperature, which meant that the selectivity to CO₂ had a maximum value of 673 K.

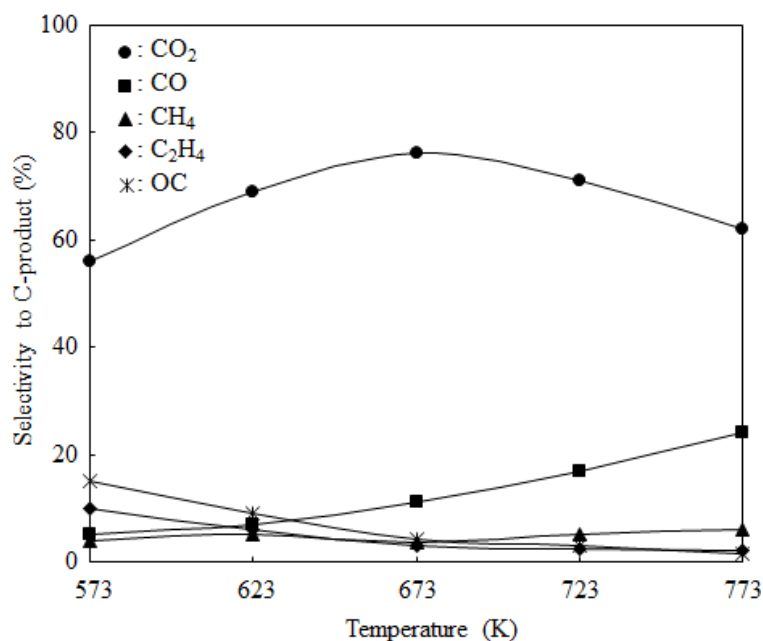


Figure 7. Effect of reaction temperature on selectivity to C-containing products over 7.7 wt. % Co/CeO₂ (hp).

Figure 8 shows the effect of reaction temperature on H₂ yield over 7.7 wt. % Co/CeO₂ (hp). The reaction conditions are the same as those in Table 2. Because the ethanol conversion increased with increasing reaction temperature, the H₂ yield increased with increasing the reaction temperature at a reaction temperature below 723 K. However, the selectivity to CO greatly increased when the ethanol conversion reached to near 100% at a reaction temperature above 723 K. The CO formation decreased the selectivity to CO₂, and thus decreased the H₂ yield for the reaction. Hence, the maximum value of H₂ yield was observed at 723 K over 7.7 wt. % Co/CeO₂ (hp).

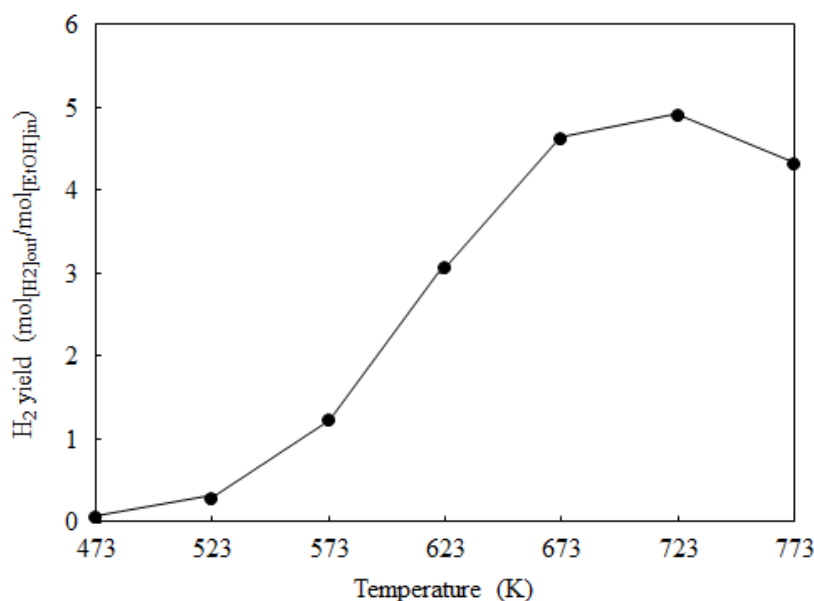


Figure 8. Effect of reaction temperature on H₂ yield over 7.7 wt. % Co/CeO₂ (hp).

2.3. Catalyst Deactivation and Regeneration

Figure 9 shows the catalyst deactivation and regeneration for ethanol steam reforming over 7.7 wt. % Co/CeO₂ (hp) at 673 K. The reaction conditions are the same as those in Table 2. Figure 9a shows the time course of ethanol steam reforming over fresh catalyst at 673 K. The catalyst showed the initial conversions of 85.9% and it decreased to 70.4% after reaction at 673 K for 120 h. As for the catalyst deactivation, there are three possible reasons: Co sintering, Co oxidation, and carbonaceous deposits. Because the CO absorption measurement indicated that the size of the Co particles did not change after reaction at 673 K for 120 h, it is unlikely that the deactivation would be caused by the sintering of the Co. The deactivated catalyst (after 120 h on stream at 673 K) was reduced by H₂ at 673 K for 10 h and then used again for the steam reforming of ethanol at 673 K. The time course was shown in Figure 9b. The catalytic activity did not recover and the initial conversion was about 70%. This indicates that the oxidation of Co is not the reason for the catalyst deactivation. Moreover, the deactivated catalyst (after 120 h on stream at 673 K) was regenerated by calcination in air at 723 K for 3 h and then reduction in H₂ flow at 673 K for 10 h. The time course was shown in Figure 9c. The catalytic activity recovered to its initial conversion of about 85%. These results indicated that the carbonaceous deposits formed on the catalyst surface caused the catalyst deactivation during the reaction.

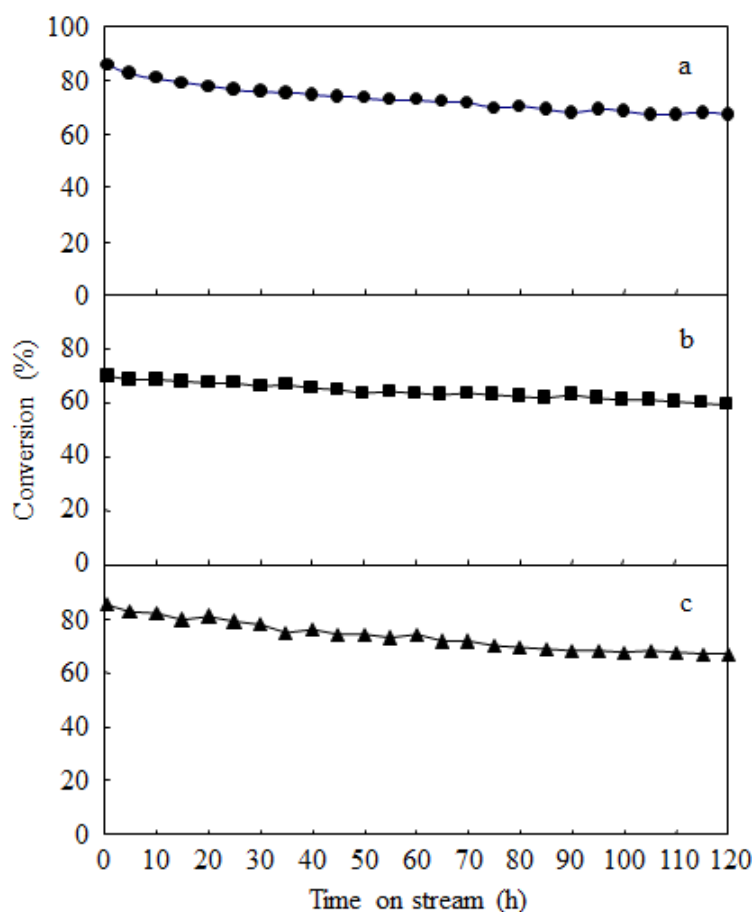


Figure 9. Catalyst deactivation and regeneration for ethanol steam reforming over 7.7 wt % Co/CeO₂ (hp) at 673 K. (a) Fresh catalyst; (b) the used catalyst (after reaction at 673 K for 120 h) was reduced by H₂ at 673 K for 10 h; (c) the used catalyst (after reaction at 673 K for 120 h) was calcined in air at 723 K for 3 h and then reduced by H₂ at 673 K for 10 h.

The amount of carbonaceous deposits on the used catalyst was calculated by a temperature programmed oxidation (TPO) method [31,32]. After testing the fresh 7.7 wt. % Co/CeO₂ (hp) catalyst at 673 K for 120 h, the reactor was filled with nitrogen and cooled to 373 K. Then, an air flow of 1.5 L·h⁻¹ was introduced in the reactor. Finally, the TPO experiment was performed by heating the reactor from 373 to 923 K with a rate of 2.5 K·min⁻¹ in the air flow. The off-gases were analysed by GC-TCD as usual. During the TPO treatment, the carbonaceous deposits formed on the catalyst surface were oxidized to CO₂ by oxygen in the air flow. The amounts of formed CO₂ were recorded by TCD at various temperatures.

Figure 10 shows the CO₂ formation from carbonaceous deposits over the 7.7 wt. % Co/CeO₂ (hp) catalyst after reaction at 673 K for 120 h. The used catalyst was treated in air (1.5 L·h⁻¹) by increasing the temperature at 2.5 K·min⁻¹. CO₂ formation was observed at above 373 K and showed two peaks with the maximum values at 523 and 673 K. An integration of the rate gave the amount of total CO₂, from which the amount of carbonaceous deposits formed on the 7.7 wt. % Co/CeO₂ (hp) catalyst was calculated as follows: 2.1 wt. % carbonaceous deposits on the surface of 7.7 wt. % Co/CeO₂ (hp) after 120 h on stream at 673 K.

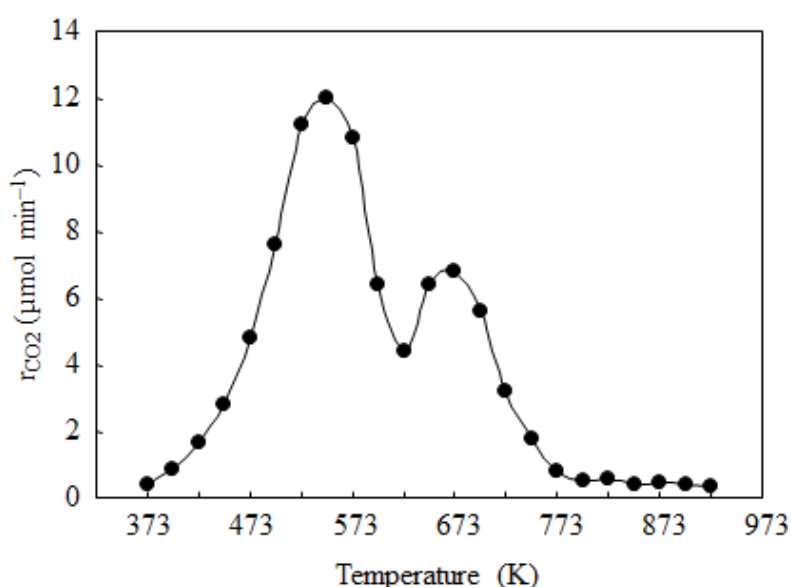


Figure 10. CO₂ formation from carbonaceous deposits over the 7.7 wt. % Co/CeO₂ (hp) catalyst after reaction at 673 K for 120 h.

There are two peaks with the highest rates of CO₂ formation at 523 K and 673 K in Figure 10, implying there were two types of carbonaceous deposits formed on the catalyst surface during the reaction. It has been reported that the ethylene and oxygen-containing molecules can contribute to the coke formation for the steam reforming of ethanol [13]. Moreover, the formation of carbon filaments on the catalyst have been confirmed in the steam reforming of ethanol [13].

The carbonaceous deposits may be mainly formed by the Boudouard reaction (Equation (9)) and the polymerization of by-product ethylene (Equation (10)).



In general, the oxidation temperature of (CH₂)_{2n} polymers is lower than that of carbon filaments. Hence, we think the peak at 523 K corresponds to the carbonaceous deposits formed from the ethylene

polymerization (Equation (10)) and the peak at 673 K corresponds to the carbonaceous deposits formed from the Boudouard reaction (Equation (9)), respectively.

3. Experimental Section

3.1. Catalyst Preparation

Co/CeO₂ (hp) was obtained through a precursor of Ce_{1-x}Co_xO_{2-y} mixed oxide by homogeneous precipitation using urea as a precipitant [26,27]. Urea was added into a mixed aqueous solution of Ce(NO₃)₃ and Co(NO₃)₂ at room temperature to form a homogeneous solution. Then, the solution was heated at 363 K and hence the urea was hydrolyzed slowly. During the hydrolysis of urea, hydroxide ions were generated and a precipitate was formed slowly. After heating the solution at 363 K for 10 h, the formed Ce_{1-x}Co_xO_{2-y} precipitate was filtered, washed with distilled water, dried in air at 373 K for 24 h and finally calcined in air at 723 K for 3 h.

Co/CeO₂ (cp) was prepared by a co-precipitation method using NaOH as a precipitant [30]. A mixed aqueous solution of Ce(NO₃)₃ and Co(NO₃)₂ was co-precipitated by adding 2 M NaOH solution till pH = 10 at room temperature. After being aged at 363 K for 1 h, the precipitate was filtered, washed with distilled water, dried at 373 K for 24 h, and finally calcined in air at 723 K for 3 h.

CeO₂, which was used as a support in the impregnation Co/CeO₂ (im) catalyst, was prepared by the precipitation of Ce(NO₃)₃ in an aqueous solution using 2 M NaOH solution as a precipitant. After being aged at 363 K for 1 h, the precipitate was filtered, washed with distilled water, dried at 373 K for 24 h, and finally calcined in air at 723 K for 3 h.

Co/CeO₂ (im) was prepared by an impregnation of the CeO₂ support with an aqueous solution of Co(NO₃)₂. The obtained solid sample was dried at 373 K for 24 h and calcined in air at 723 K for 3 h.

Co/Al₂O₃ (im) was prepared by an impregnation of the Al₂O₃ support (JRC-ALO-4, 167 m²·g⁻¹) with an aqueous solution of Co(NO₃)₂. The obtained solid sample was dried at 373 K for 24 h and calcined in air at 723 K for 3 h.

3.2. Catalyst Characterization

Powder X-ray diffraction (XRD) patterns were measured using a MAC Science MXP-18 diffractometer (Tokyo, Japan) with Cu K α radiation operated at 40 kV and 50 mA. Inductively coupled plasma (ICP) analyses were measured by a Thermo Jarrel Ash IRIS/AP (Yokohama, Japan). BET surface areas of the samples were measured using a BELCAT-B automatic instrument (Osaka, Japan). Transmission electron microscopy (TEM) images were obtained using a JEOL JEM 2010FX electron microscope (Tokyo, Japan) equipped with a Hitachi/Keves H-8100/Delta IV EDS (Tokyo, Japan) operating at 200 kV. The *ex situ* treated samples were supported on Mo grids for the observations. The Co particle sizes of the Co supported catalysts were measured by a CO adsorption method using a flow technique at room temperature [39,40,42,43]. A 0.3 g portion of sample was reduced in a flow H₂ at 673 K for 10 min and then used for the measurements. The particle size of Co (D) was calculated by the relations of $S = \alpha NS'$ and $D = 6/\rho S$, where S the metal surface area of Co (m²·g⁻¹ Co), α is the amount of CO adsorbed (mol·g⁻¹ Co), N the Avogadro's number, S' is the cross-sectional area of a CO molecule (13 Å), and ρ is the specific gravity of Co. Hydrogen temperature-programmed reduction (H₂-TPR) was recorded using a BELCAT-B automatic instrument equipped with a TCD and a mass spectrometer. The sample (ca. 0.15 g) was flushed with Ar at 423 K for 1 h in a quartz tubular reactor to drive away water and then cooled down to 373 K. Then, 10% H₂/Ar was switched on at a flow rate of 30 mL·min⁻¹. The temperature was raised at a rate of 10 K·min⁻¹ from 373 to 873 K and was held at the final temperature for 30 min. The H₂ consumption was detected by TCD and was recorded automatically by a PC.

3.3. Catalytic Reaction

The catalytic reaction was conducted under atmospheric pressure using a fixed-bed flow system equipped with an 8 mm ϕ quartz tubular reactor. An ethanol aqueous solution was fed from a tank by a high-pressured micro-pump (Shimadzu LC-10, Kyoto, Japan) to the reactor set at the reaction temperature. At the same time, nitrogen was also introduced into the reactor from a gas cylinder as a carry gas. The inlet gas contained 20% ethanol, 60% steam and 20% nitrogen. During reaction, the flow rates of ethanol, steam and nitrogen were 17, 50, and 17 mL \cdot min $^{-1}$, respectively. The catalyst amount was one gram for the reaction, and thus the total gas hourly space velocity (GHSV) was 5000 mL \cdot h $^{-1}\cdot$ g $^{-1}$.

The steam reforming of ethanol was mainly carried out at 673 K over various catalysts in this study. Calcination and reduction of a Co-supported catalyst at a high temperature must cause a severe sintering of Co particles and a remarkable decrease of BET surface area. We calcined the catalysts at 723 K for 3 h in this study in order to maintain relatively large BET surface areas. Moreover, we reduced the catalysts in H₂ flow at a low temperature (673 K, the same as reaction temperature) for a long time (10 h) in this study in order to avoid the sintering of Co particles.

The reaction was started after the catalyst (1 g, 60 meshes) was pretreated in a H₂ flow (50 mL \cdot min $^{-1}$) at 673 K for 10 h. The products were analyzed using three on-line gas chromatographs. H₂, N₂, CO, and CO₂ were analyzed by a TCD (Shimadzu, Kyoto, Japan) with a New Carbon-ST column (Shinwa Chem. Ind. Ltd., Kyoto, Japan), hydrocarbons were analyzed by an FID (Shimadzu, Kyoto, Japan) with a CP-Al₂O₃/KCl capillary column (Agilent Technologies Inc., Santa Clara, CA, USA), and oxygenated compounds were analyzed by an FID with a Stablewax capillary column (Restek Co., Bellefonte, PA, USA).

The ethanol conversion was reported as a percent conversion: $C_{\text{EtOH}} = ([\text{EtOH}]_{\text{in}} - [\text{EtOH}]_{\text{out}})/[\text{EtOH}]_{\text{in}} \times 100$. The selectivity of each carbon-containing product was reported as a percent selectivity: $S_{\text{product}} = [\text{product}]/\Sigma[\text{product}] \times 100$. The yield of hydrogen was reported as a molar ratio of the formed H₂ to the fed C₂H₅OH: $Y_{\text{H}_2} = [\text{H}_2]_{\text{out}}/[\text{EtOH}]_{\text{in}}$. The analytical results satisfied the carbon balance adequately ($<\pm 5\%$).

4. Conclusions

The Co/CeO₂ (hp) catalyst showed a higher catalytic activity than those over Co/CeO₂ (cp) and Co/CeO₂ (im) for the steam reforming of ethanol because Co/CeO₂ (hp) had a larger BET surface area and smaller Co particles. The ethanol conversion reached its maximum value at 17.4 wt. % Co loading, but the TOF value greatly decreased at Co loading greater than 7.7 wt. % in the Co/CeO₂ (hp) catalyst for the steam reforming of ethanol at 673 K. The selectivity to CO₂ reached its maximum value at 673 K and the yield of H₂ reached its maximum value at 723 K for the steam reforming of ethanol over 7.7 wt. % Co/CeO₂ (hp). About 2.1 wt. % carbonaceous deposits was formed on the surface of 7.7 wt. % Co/CeO₂ (hp) after reaction at 673 K for 120 h. The carbonaceous deposits caused a slow catalyst deactivation in the steam reforming of ethanol at 673 K. The deactivated catalyst could be regenerated by calcination in air at 723 K for 3 h and then reduction in H₂ flow at 673 K for 10 h.

Author Contributions: Y.L. conceived and designed the experiments, Y.L. performed the experiments, Y.L., K.M. and M.I. analyzed the data, Y.L. drafted the paper. All authors have given approval for the final version of the manuscript.

Conflicts of Interest: The authors declare no conflict of interest.

References

1. Ioannides, T. Thermodynamic Analysis of Ethanol Processors for Fuel Cell Applications. *J. Power Sources* **2001**, *92*, 17–25. [[CrossRef](#)]
2. Ni, M.; Leung, D.T.C.; Leung, K.H. A Review on Reforming Bio-Ethanol for Hydrogen Production. *Int. J. Hydrogen Energy* **2007**, *32*, 3238–3247. [[CrossRef](#)]

3. Sun, J.; Qiu, X.; Wu, F.; Zhu, W.; Wang, W.; Hao, S. Hydrogen from Steam Reforming of Ethanol in Low and Middle Temperature Range for Fuel Cell Application. *Int. J. Hydrogen Energy* **2004**, *29*, 1075–1081. [[CrossRef](#)]
4. Cifuentes, B.; Valero, M.F.; Conesa, J.A.; Cobo, M. Hydrogen Production by Steam Reforming of Ethanol on Rh–Pt Catalysts: Influence of CeO₂, ZrO₂, and La₂O₃ as Supports. *Catalysts* **2015**, *5*, 1872–1896. [[CrossRef](#)]
5. Calles, J.A.; Carrero, A.; Vizcaíno, A.J.; Lindo, M. Effect of Ce and Zr Addition to Ni/SiO₂ Catalysts for Hydrogen Production through Ethanol Steam Reforming. *Catalysts* **2015**, *5*, 58–76. [[CrossRef](#)]
6. Vargas, J.C.; Ivanova, S.; Thomas, S.; Roger, A.-C.; Pitchon, V. Influence of Gold on Ce–Zr–Co Fluorite-Type Mixed Oxide Catalysts for Ethanol Steam Reforming. *Catalysts* **2012**, *2*, 121–138. [[CrossRef](#)]
7. Domínguez, M.; Taboada, E.; Molins, E.; Llorca, J. Co–Fe–Si Aerogel Catalytic Honeycombs for Low Temperature Ethanol Steam Reforming. *Catalysts* **2012**, *2*, 386–399. [[CrossRef](#)]
8. Llorca, L.; Homs, N.; Sales, J.; Fierro, J.G.; Piscina, P.R. Effect of Sodium Addition on the Performance of Co–ZnO-based Catalysts for Hydrogen Production from Bioethanol. *J. Catal.* **2004**, *222*, 470–480. [[CrossRef](#)]
9. Haga, F.; Nakajima, T.; Miya, H.; Mishima, S. Catalytic Properties of Supported Cobalt Catalysts for Steam Reforming of Ethanol. *Catal. Lett.* **1997**, *48*, 223–237. [[CrossRef](#)]
10. Llorca, J.; Dalmon, J.A.; Piscina, P.R.; Homs, N. *In Situ* Magnetic Characterisation of Supported Cobalt Catalysts under Steam-Reforming of Ethanol. *Appl. Catal. A* **2003**, *243*, 261–269. [[CrossRef](#)]
11. Tuti, S.; Pepe, F. On the Catalytic Activity of Cobalt Oxide for the Steam Reforming of Ethanol. *Catal. Lett.* **2008**, *122*, 196–203. [[CrossRef](#)]
12. Urasaki, K.; Tokunaga, K.; Sekine, Y.; Kikuchi, E.; Matsukata, M. Hydrogen Production by Steam Reforming of Ethanol using Cobalt and Nickel Catalysts Supported on Strontium Titanate. *Chem. Lett.* **2005**, *34*, 668–669. [[CrossRef](#)]
13. Bichon, P.; Haugom, G.; Venvik, H.J.; Holmen, A.; Blekkan, E.A. Steam Reforming of Ethanol over Supported Co and Ni Catalysts. *Top. Catal.* **2008**, *49*, 38–45. [[CrossRef](#)]
14. Sun, J.; Qiu, X.; Wu, F.; Zhu, W. H₂ from Steam Reforming of Ethanol at Low Temperature over Ni/Y₂O₃, Ni/La₂O₃ and Ni/Al₂O₃ Catalysts for Fuel-Cell Application. *Int. J. Hydrogen Energy* **2005**, *30*, 437–445. [[CrossRef](#)]
15. Deng, X.; Sun, J.; Yu, S.; Xi, J.; Zhu, W.; Qiu, X. Steam Reforming of Ethanol for Hydrogen Production over NiO/ZnO/ZrO₂ Catalysts. *Int. J. Hydrogen Energy* **2008**, *33*, 1008–1013. [[CrossRef](#)]
16. Biswas, P.; Kunzru, D. Steam Reforming of Ethanol for Production of Hydrogen over Ni/CeO₂–ZrO₂ Catalyst: Effect of Support and Metal Loading. *Int. J. Hydrogen Energy* **2007**, *32*, 969–980. [[CrossRef](#)]
17. Biswas, P.; Kunzru, D. Steam Reforming of Ethanol on Ni–CeO₂–ZrO₂ Catalysts: Effect of Doping with Copper, Cobalt and Calcium. *Catt. Lett.* **2007**, *118*, 36–49. [[CrossRef](#)]
18. Ye, J.L.; Wang, Y.Q.; Liu, Y.; Wang, H. Steam Reforming of Ethanol over Ni/Ce_xTi_{1–x}O₂ Catalysts. *Int. J. Hydrogen Energy* **2008**, *33*, 6602–6611. [[CrossRef](#)]
19. Zhang, B.; Cai, W.; Li, Y.; Xu, Y.; Shen, W. Hydrogen Production by Steam Reforming of Ethanol over an Ir/CeO₂ Catalyst: Reaction Mechanism and Stability of the Catalyst. *Int. J. Hydrog. Energy* **2008**, *33*, 4377–4386. [[CrossRef](#)]
20. Diagne, C.; Idriss, H.; Kiennemann, A. Hydrogen Production by Ethanol Reforming over Rh/CeO₂–ZrO₂ Catalysts. *Catal. Commun.* **2002**, *3*, 565–571. [[CrossRef](#)]
21. Scott, M.; Goeffroy, M.; Chiu, W.; Blackford, M.A.; Idriss, H. Hydrogen Production from Ethanol over Rh–Pd/CeO₂ Catalysts. *Top. Catal.* **2008**, *51*, 13–21. [[CrossRef](#)]
22. Platon, A.; Roh, H.S.; King, D.L.; Wang, Y. Deactivation Studies of Rh/Ce_{0.8}Zr_{0.2}O₂ Catalysts in Low Temperature Ethanol Steam Reforming. *Top. Catal.* **2007**, *46*, 374–379. [[CrossRef](#)]
23. Roh, H.S.; Wang, Y.; King, D.L. Selective Production of H₂ from Ethanol at Low Temperatures over Rh/ZrO₂–CeO₂ Catalysts. *Top. Catal.* **2008**, *49*, 32–37. [[CrossRef](#)]
24. Aupretre, F.; Descorme, C.; Duprez, D. Bio-Ethanol Catalytic Steam Reforming over Supported Metal Catalysts. *Catal. Commun.* **2002**, *3*, 263–267. [[CrossRef](#)]
25. Cavallaro, S. Ethanol Steam Reforming on Rh/Al₂O₃ Catalysts. *Energy Fuels* **2000**, *14*, 1195–1199. [[CrossRef](#)]
26. Shishido, T.; Yamamoto, Y.; Morioka, H.; Takaki, H.; Takehira, K. Active Cu/ZnO and Cu/ZnO/Al₂O₃ Catalysts Prepared by Homogeneous Precipitation Method in Steam Reforming of Methanol. *Appl. Catal. A* **2004**, *263*, 249–453. [[CrossRef](#)]

27. Shishido, T.; Yamamoto, M.; Li, D.; Tian, Y.; Morioka, H.; Honda, M.; Sano, T.; Takehira, K. Water-Gas Shift Reaction over Cu/ZnO and Cu/ZnO/Al₂O₃ Catalysts Prepared by Homogeneous Precipitation. *Appl. Catal. A* **2006**, *303*, 62–71. [[CrossRef](#)]
28. Hayakawa, T.; Harihara, H.; Andersen, A.G.; York, A.; Suzuki, K.; Yasuda, H.; Takehira, K. A Sustainable Catalyst for the Partial Oxidation of Methane to Syngas: Ni/Ca_{1-x}Sr_xTiO₃, Prepared *in Situ* from Perovskite Precursors. *Angew. Chem. Int. Ed.* **1996**, *35*, 192–195. [[CrossRef](#)]
29. Liu, Y.; Suzuki, K.; Hamakawa, S.; Hayakawa, T.; Murata, K.; Ishii, T.; Kumagai, M. Catalytic Methanol Decomposition at Low Temperature over Pd Catalyst Derived from Mesoporous Silica Carried Pd-Hydrotalcite. *Chem. Lett.* **2000**, *29*, 486–487. [[CrossRef](#)]
30. Liu, Y.; Suzuki, K.; Hamakawa, S.; Hayakawa, T.; Murata, K.; Ishii, T.; Kumagai, M. Highly Active Methanol Decomposition Catalyst Derived from Pd-Hydrotalcite Dispersed on Mesoporous Silica. *Catal. Lett.* **2000**, *66*, 205–213. [[CrossRef](#)]
31. Liu, Y.; Hayakawa, T.; Suzuki, K.; Hamakawa, S. Production of Hydrogen by Steam Reforming of Methanol over Cu/CeO₂ Catalysts Derived from Ce_{1-x}Cu_xO_{2-x} Precursors. *Catal. Commun.* **2001**, *2*, 195–200. [[CrossRef](#)]
32. Liu, Y.; Hayakawa, T.; Suzuki, K.; Hamakawa, S.; Tsunoda, T.; Ishii, T.; Kumagai, M. High Active Copper/Ceria Catalysts for the Steam Reforming of Methanol. *Appl. Catal. A Gen.* **2002**, *223*, 137–145. [[CrossRef](#)]
33. Liu, Y.; Hayakawa, T.; Ishii, T.; Kumagai, M.; Yasuda, H.; Suzuki, K.; Hamakawa, S.; Murata, K. Methanol Decomposition to Synthesis Gas at Low Temperature over Palladium Support on Ceria-Zirconia Solid Solutions. *Appl. Catal. A* **2001**, *210*, 301–314. [[CrossRef](#)]
34. Liu, Y.; Hayakawa, T.; Tsunoda, T.; Suzuki, K.; Hamakawa, S.; Murata, K.; Shiozaki, R.; Ishii, T.; Kumagai, M. Steam Reforming of Methanol over Cu/CeO₂ Catalysts Studied in Comparison with Cu/ZnO and Cu/Zn(Al)O Catalysts. *Top. Catal.* **2003**, *22*, 205–213. [[CrossRef](#)]
35. Liu, Y.; Murata, K.; Hanaoka, T.; Inaba, M.; Sakanishi, K. Syntheses of New Peroxo-Polyoxometalates Intercalated Layered Double Hydroxides for Propene Epoxidation by Molecular Oxygen in Methanol. *J. Catal.* **2007**, *248*, 277–287. [[CrossRef](#)]
36. Liu, Y.; Murata, K.; Inaba, M.; Takahara, I.; Okabe, K. Synthesis of Mixed Alcohols from Syngas over Cs-Modified Cu/Ce_{1-x}Zr_xO₂ Catalysts. *J. Jpn. Pet. Inst.* **2010**, *53*, 153–159. [[CrossRef](#)]
37. Liu, Y.; Murata, K.; Inaba, M.; Takahara, I.; Okabe, K. Synthesis of Ethanol from Syngas over Rh/Ce_{1-x}Zr_xO₂ Catalysts. *Catal. Today* **2011**, *164*, 308–314.
38. Liu, Y.; Murata, K.; Inaba, M.; Takahara, I.; Okabe, K. Mixed Alcohols Synthesis from Syngas over Cs- and Ni-Modified Cu/CeO₂ Catalysts. *Fuel* **2013**, *104*, 62–69. [[CrossRef](#)]
39. Liu, Y.; Hanaoka, T.; Miyazawa, T.; Murata, K.; Okabe, K.; Sakanishi, K. Fischer-Tropsch Synthesis in Slurry-phase Reactors over Mn- and Zr-Modified Co/SiO₂ Catalysts. *Fuel Process. Technol.* **2009**, *90*, 901–908. [[CrossRef](#)]
40. Liu, Y.; Murata, K.; Okabe, K.; Hanaoka, T.; Sakanishi, K. Synthesis of Zr-Grafted SBA-15 as an Effective Support for Cobalt Catalyst in Fischer-Tropsch Synthesis. *Chem. Lett.* **2008**, *37*, 984–985. [[CrossRef](#)]
41. Fan, L.; Fujimoto, K. Reaction Mechanism of Methanol Synthesis from Carbon Dioxide and Hydrogen on Ceria-Supported Palladium Catalysts with SMSI Effect. *J. Catal.* **1997**, *172*, 238–242. [[CrossRef](#)]
42. Sun, S.; Tsubaki, N.; Fujimoto, K. The Catalytic Performance and Characterization of Fischer-Tropsch Synthesis Co/SiO₂ Catalysts Prepared from Mixed Cobalt Salts. *Appl. Catal. A* **2000**, *202*, 121–131. [[CrossRef](#)]
43. Sun, S.; Fujimoto, K.; Yoneyama, Y.; Tsubaki, N. Fischer-Tropsch Synthesis Using Co/SiO₂ Catalysts Prepared from Mixed Precursors and Addition Effect of Noble Metal Salts. *Fuel* **2002**, *81*, 1583–1591. [[CrossRef](#)]

